SciMedCentral

JSM Environmental Science & Ecology

Research Article

Enhancing the Quality of Satellite Images for Estimating the Water Body

Mohammad Roohi*

Department of Civil Engineering, Shahid Chamran University of Ahvaz, Ahvaz, Iran

***Corresponding author**
Mohammad Roohi, Department of Civil Engineering, Shahid Chamran University of Ahvaz, Ahvaz, Iran

Submitted: 06 January, 2024

Accepted: 26 January, 2024

Published: 29 January, 2024

ISSN: 2333-7141

Keywords

- Dam Lake; Landsat-8; Remote Sensing; Image Fusion

Abstract

Water resources are indeed limited, and factors such as drought, climate change, and human activities can contribute to their decrease. To estimate the amount of water stored in a dam lake, several methods can be employed. Remote sensing techniques, such as satellite imagery can be used to estimate the water surface area of the reservoir. In this study, the amount of water cover changes is investigated using a remote sensing technique. Also, to increase the level of accuracy in estimating the water cover of the dam lake, the technique of Image Fusion Landsat-8 satellites images and increasing the level of spatial accuracy from 30 meters to 15 meters has been used. In this study, it has been shown that by combining Landsat satellite images, the accuracy in calculating and estimating the water cover area has increased. Also, in this study, the depth changes between 2017-2020 have been investigated. In the research conducted, the amount of water stored in the dam lake has decreased due to the droughts of the last few years, due to the increase in water consumption in the urban and agricultural areas, especially during the drought period.

INTRODUCTION

Rivers and lakes form an important part of the hydrological cycle of water and are an important source of life on earth. Surface water, as the most important land resource, undergoes spatial and temporal changes and includes many factors such as land use changes, land cover level, climate changes, seasonal changes, and environmental changes that occur all over the world [1-3]. Earth's water levels are one of the irreplaceable (non-renewable) strategic resources for human survival. Nowadays, the use of satellite images and remote sensing technology has become very practical due to the reduction of time, and cost, the possibility of performing various location-based processes and repeatability in different seasons and times, and plays a key role in monitoring wetlands, flood assessment, and level estimation. Water zones and water resources management. One of the most important sources of water storage in the world is the dam, which has an important contribution to the distribution of the amount of water stored in it, therefore, accurate information on the amount of water coverage in the dam lake and the amount of water stored in it is very important. Mapping and monitoring of water resources is a necessary condition for access, use, and better management of water resources in arid and semi-arid regions [4].

Reservoir dams, are artificial lakes created by humans for specific purposes, the name lake is also applied to reservoirs for the reason that reservoirs can be described as a volume of water with a special composition, in which different species of Life flow it. Of course, there are many differences between natural lakes and reservoirs of dams. Unlike natural lakes that are formed in the lowland areas of the watershed, dam reservoirs are usually created in river valleys by constructing dams along the river flow [5,6]. The increase in wavelength of water radiation tends to zero, and this feature allows us to easily separate it from other phenomena by using different indicators. Indicators are made by combining two or more different bands and using the difference between the spectral range of these bands improves the received spectral signal, better identification, and removes noise from different parts of the wavelengths [7]. In the past decades, a wide range of depth calculation algorithms has been developed, whose purpose is to calculate the water depth by remote sensing based on the physical relationships of the corresponding wave parameters. These algorithms estimate the water depth by taking wave images from radar and video [8,9], or data modeling from video integration, observation of the separation of wave patterns [10,11]. Accurate estimation of areas with shallow water depth is important for the navigation safety of small boats such as fishing boats and fundamental studies [12].

Remote sensing is a very suitable and effective solution due to its high ability to collect information in a short time and in wide ranges with the ability to calculate indicators related to hydrological studies [13,14]. The data obtained from the sensors installed on the Landsat series of satellites are one of the most important sources of information for the preparation of land use maps, land cover, and water areas [15,16]. The last generation of these satellites, which is called Landsat 8, was launched on February 11, 2013, and has two sensors called OLI and TIRS. Improving the radiometric resolution of the OLI meter to 16 bits has made it possible to conduct some studies, especially in the field of preparing a distribution map of various types of vegetation [17]. The characteristics of water from satellite

images are analyzed using different indices such as Normalized Vegetation Index (NDVI), Normalized Water Cover Index (NDWI), and modified normalized water cover index [18-20]. In past research, the MNDWI index has obtained more favorable results for water extraction from Landsat, Spot, Aster, and MODIS satellite images [7,21]. Dennison, et al. 2005. They concluded that the NDWI index has little sensitivity to vegetation that has a large amount of water in them. The mentioned indicators are in the numerical range between 1 and -1. However, the definition of a threshold limit and a specific number for water detection are different according to the characteristics of the water and the coverage of the area.

Fusion of satellite images means the integration of satellite images. By using this work, it is possible to merge images with a high spatial resolution (for example, the panchromatic band of a satellite image with high spatial resolution) and a multispectral image with high spectral resolution (for example, color combination 2, 4, 3 of the Landsat image). And create a new image with better spatial resolution and high spectral resolution (due to maintaining the value of existing pixels) and be able to extract better and more data from the new image [7]. In the method of Fusion satellite images using the Gram-Schmidt method, a panchromatic band with a high spatial resolution is simulated with bands that have a lower spatial quality. In the next step, conversion and transmission are done to simulate the panchromatic band, and the MS bands are obtained with the panchromatic simulation band as the first band. Then the panchromatic band with high spatial power replaces the band with a lower resolution [22]. In this study, by using Landsat 8 satellite images and image fusion, the spatial resolution of the images has increased. Also, the amount of water cover area and water depth changes behind Mamloo dam lake have been calculated. The amount of dispersion of water cover between the years 2017 and 2020 and the changes in the area of water depth for four modes of very shallow, shallow, medium, and deep have been investigated, and finally, the decrease in the amount of water area due to the droughts of the last few years. Has been analyzed.

MATERIALS AND METHODS

Study Area

Mamloo Dam (Darwazah) is built in the province of Tehran, 30 km southeast of Tehran, with a geographic location of 35.585 degrees north and 51.788 degrees east, on the Jajroud river and the seasonal Damavand River in Mamloo village. The purpose of the construction of Mamloo dam is to supply agricultural water, drinking water, and electricity to the cities of Pakdasht, Varamin, and south of Tehran. The lake of this dam is about 800 meters wide and 3000 meters long. The type of dam is earthen with a clay core, its height from the foundation is 89 meters, the length of its crown is 807 meters, and the volume of its reservoir is 250 million cubic meters. Dams in this region play a vital role in water resource management, especially in supplying water for agriculture, domestic use, and supporting the ecosystems. They help in regulating water flow, providing water storage during periods of high precipitation, and releasing water during drier periods [23].

Dataset

In this study, Landsat 8 satellite images of OLI sensor were used. The received images are in the period of 2017-2020. The way to get and download images is from https://earthexplorer.usgs.gov/, which images are available for free. Landsat 8, officially known as the Landsat Data Continuity Mission (LDCM), was launched on February 11, 2013. It was a joint effort between NASA and the United States Geological Survey (USGS). The satellite was launched aboard an Atlas V rocket from Vandenberg Air Force Base in California, USA. Landsat 8 is part of the long-running Landsat program, which has been capturing images of the Earth's surface since 1972. It carries the Operational Land Imager (OLI) and the Thermal Infrared Sensor (TIRS), which provide valuable data for monitoring land use, natural resources, and environmental changes. The satellite orbits the Earth in a polar sun-synchronous orbit, which means it passes over the same area at the same local solar time on each orbit [24].

Pre-processing of Satellite Images

Radiometric calibration: The data obtained from remote sensing systems, including aerial photographs and images obtained from scanners (satellite images), have various errors and must be corrected before being interpreted and analyzed. These errors can be divided into two categories: geometric and radiometric. Geometric errors are related to the position of phenomena or pixels in the image relative to other phenomena and their absolute position, and radiometric error is related to the amount of reflection recorded in the image. Radiometric calibration is the process of converting the raw sensor measurements from a satellite or remote sensing instrument into meaningful and accurate radiometric values. It involves removing the systematic errors, variations, and biases in the sensor data to ensure the consistency and reliability of the measurements. Also, shadow or radiometric calibration can be used to reduce the effects of surface reflection reduction [25-27]. First, we include radiometric calibrations on the images. Using radiometric calibrations, radiance values (amount of energy reaching the sensor), which is the most accurate parameter estimated in RS, are calculated for MS bands, which is a background for atmospheric correction. The radiance values obtained from equation one is linear and very simple and are estimated [28].

$$Y = ax + b \qquad (1)$$

In this equation, Y is equal to the radiance value, X is equal to the Digit Number (DN) image (the original images that we downloaded), a, whose value is included in the metadata file named Radiance-Multi-Band for each band, and b, which is named Radiance-Add - Band is available in the metadata file.

Atmospheric corrections: Atmospheric correction is a crucial step in the processing of satellite imagery or remote

sensing data to account for the influence of the Earth's atmosphere on the measured electromagnetic radiation. The atmosphere interacts with the incoming solar radiation and affects the signal received by the satellite sensor, leading to errors in the interpretation of the data. Atmospheric correction aims to remove these atmospheric effects and obtain accurate surface reflectance or radiance values [29]. Atmospheric correction typically requires information about atmospheric conditions such as aerosol content, water vapor, and ozone concentrations. This information can be derived from ancillary data sources like meteorological measurements, atmospheric models, or satellite-based atmospheric sensors. Atmospheric correction is described in equation 2 [28].

$$L_s = L_t + L_p \qquad (2)$$

In this equation, Ls is the energy recorded by the meter, Lt is the energy emitted from the earth's surface, and Lp is the effects of the atmosphere on electromagnetic waves. In the atmospheric correction, we intend to completely remove the Lp factor. The effect of the atmosphere on the path of electromagnetic waves should be completely removed and the value of Ls = Lt. This is all the operation we intend to do in atmospheric correction. In this study, atmospheric corrections have been made using the Quick Atmosphere Correction algorithm. The image that is obtained after atmospheric correction actually shows the images of surface reflections which physically, the values of this image should be between 0 and 1.

Image Fusion

Image fusion, also known as data fusion or image integration, is the process of combining multiple images of the same scene or area acquired from different sensors or sources to create a single composite image that incorporates the complementary information from each source. The goal of image fusion is to enhance the overall quality, clarity, and interpretability of the resulting image by leveraging the strengths of each input image. The specific choice of fusion technique and satellite sensors depends on the application and the desired outcome. Different fusion algorithms, such as pixel-level, feature-level, or decision-level fusion, can be applied to satellite imagery to achieve the desired enhancements and information integration [30]. Satellite image fusion techniques are suitable for when we need more spatial details and more accurate separation of classes on the ground. By using fusion, the amount of spatial detail increases in real terms, and the number of mixed pixels in it decreases significantly (Figure 1). The reduction of mixed pixels allows more accurate detection of the boundaries of phenomena and increases the accuracy of spatial and spectral calculations [31]. In this study, the Gram-Schmidt algorithm was used to increase the power of spatial resolution and to convert MS bands from 30 meters to 15 meters (Figure 2). The Gram-Schmidt algorithm, this method is one of the methods of fusion of multispectral images. In this algorithm, the panchromatic band is first simulated using multispectral bands and combined with other bands. Then, a Gram-Schmidt transformation is applied to the multi-band image, which is created according to the number of integrated bands of the component. In the next step, by replacing the first component of this image with the main panchromatic band, fusion is done [32].

Modified Normalized Difference Water Index (MNDWI)

Among the most important spectral indices of water, we can mention two indices, NDWI and MNDWI, which are widely used in water detection. Xu 2006, concluded that the NDWI index is not able to eliminate the signal from built-up surfaces and the use of a threshold of 0 is not able to accurately detect surfaces composed of water pixels. Therefore, he proposed another index, called the MNDWI index, with the difference that this index can exclude other phenomena other than water and is very effective for detecting water areas. How get the MNDWI index is based on the following equation:

$$MNDWI = \frac{Green - MIR}{Green + MIR} \qquad (3)$$

Where:

- Green represents the spectral band sensitive to green vegetation reflectance (e.g., Landsat bands 3 or Sentinel-2 band 3).
- MIR refers to the shortwave infrared spectral band (e.g., Landsat bands 6 or Sentinel-2 band 11), which is sensitive to water reflectance.

The MNDWI ranges from -1 to 1, with higher values indicating the presence of water. Here's how the index works [33]:

1) Water has a high reflectance in the near-infrared portion of the electromagnetic spectrum and absorbs strongly in the shortwave infrared region. This results in a high MIR value and a low Green value in the formula, leading to positive MNDWI values.

2) Vegetation and other land features generally have high reflectance in both the green and near-infrared regions. As a result, the Green and SWIR values are comparable, leading to a lower MNDWI value or even negative values.

It's worth noting that the specific threshold value for water detection may vary depending on the satellite data, the study area, and the desired level of accuracy. Additionally, atmospheric correction and image preprocessing are typically performed before calculating the MNDWI to account for atmospheric effects and enhance the quality of the water detection results.

Water Depth Changes

Satellite imagery can be utilized to monitor water depth changes in various water bodies, including lakes, rivers, and coastal areas. By comparing satellite images acquired at different times, it is possible to observe and analyze alterations in water depth over specific periods [34].

Here's a general approach for assessing water depth changes using satellite images [35].

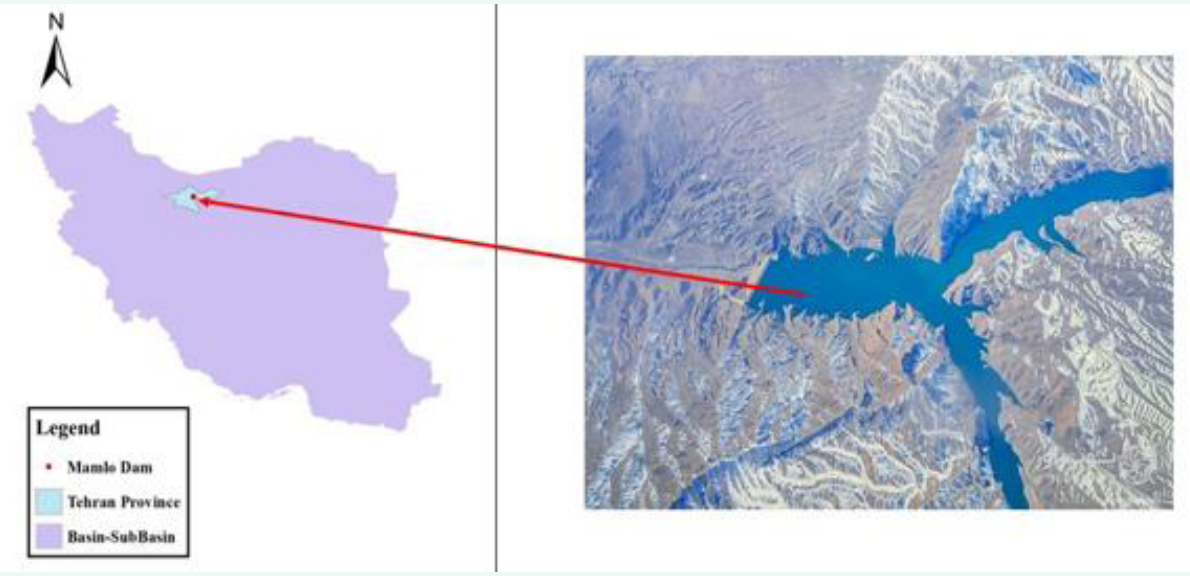

Figure 1 Study site (Mamloo dam).

Figure 2 The image on the left is the original 30-meter Landsat 8 image and the image on the right is the 15-meter fusion image with the Gram Schmidt method.

A. Acquire satellite imagery: Obtain satellite images covering the target water body at multiple time points. Ideally, these images should have consistent spatial resolution, spectral bands, and atmospheric conditions to ensure accurate comparisons.

B. Preprocess the images: Apply necessary preprocessing steps to the images to account for factors like atmospheric effects, radiometric calibration, and geometric correction. This helps to ensure the images are geometrically aligned and suitable for accurate analysis.

C. Extract water boundaries: Using image processing techniques, delineate the water boundaries in each image. This can be achieved through methods such as

thresholding, classification, or edge detection algorithms to separate water pixels from land or other features.

In this study, water depth changes from 2017 to 2020 have been investigated in four modes: very shallow, shallow, medium, and deep. (Figure 3) shows the amount of water depth changes for 2018 for the summer and autumn periods.

RESULTS AND DISCUSSION

After separating the water area of the dam lake using the MNDWI index, the area of the water body has been calculated in the summer and winter months from 2017 to 2020. With using image processing techniques, extracted the water body area by segmenting the connected water pixels and eliminating any noise or small water bodies. the results of which are given in (Table 1). According to (Table 1), the backwater area of the lake has been obtained using the MNDWI index, which separates the water area from other effects such as soil, vegetation, and humidity. According to this index, it has isolated only the places where there was a water zone and removed other effects such as wet soil. According to the research conducted [7,36-38], this index has a higher accuracy in estimating the blue area than the other indices, and the reason for this is the removal of other effects other than water from the pixels of the images. (Figure 4) shows the location of the amount of water behind the dam as seen in the figure. The location of the blue zone varies in the summer and winter seasons. Due to the droughts of the last few years and low rainfall, especially in spring and summer, the amount of water has decreased, especially behind the dam wall. The largest decrease in the area of the water area is related to September 24, 2018, when the amount of the dam lake area is 1.5651 square kilometers, which is a 69% decrease compared to the summer of 2017.09.11 when its value was 5.1050 square kilometers. He pointed out a sharp decrease in rainfall, and an increase in consumption in the agricultural and urban areas, including drinking water and other cases. (Table 2) shows the increase and decrease of the water area compared to last year in two periods of drought and drought. In (Figure 5), the value of water zone changes in summer and winter from 2017 to 2020 is shown.

The decrease in area of the blue zone in the summer of 2020 decreased by 22.5% compared to the corresponding month of 2019, and also by 60.5% compared to the corresponding month of 2018, and finally by 24% compared to the corresponding month of 2017. There has been a decrease in the blue zone. Also, in the winter period of 2020, compared to the corresponding month in 2017, there has been a decrease of 6.5%. The water area in 2020 has decreased by 18.7% compared to the corresponding month of 2018, and the water area of the dam lake in 2020 has decreased by 23.4% compared to the corresponding month in 2019. As shown in (Table 1), the largest water area in the winter of 2019 and in the summer of 2017 is due to the good rains in winter and spring, and the amount of water storage was somewhat appropriate. As it is clear in (Figure 5), the largest number of changes in the water area is related to the date 2018.09.24, which is the lowest amount of water area. The graph of the blue zone has more fluctuations

Table 1: Lake area behind the dam from 2017 to 2020.

NO	Date	Water Body are (Km^2)
1	2017.09.06	5.2134
2	2017.11.25	5.4794
3	2018.09.24	1.5651
4	2018.11.14	6.2991
5	2019.09.11	5.105
6	2019.11.14	6.6856
7	2020.09.14	3.9600
8	2020.11.17	5.1212

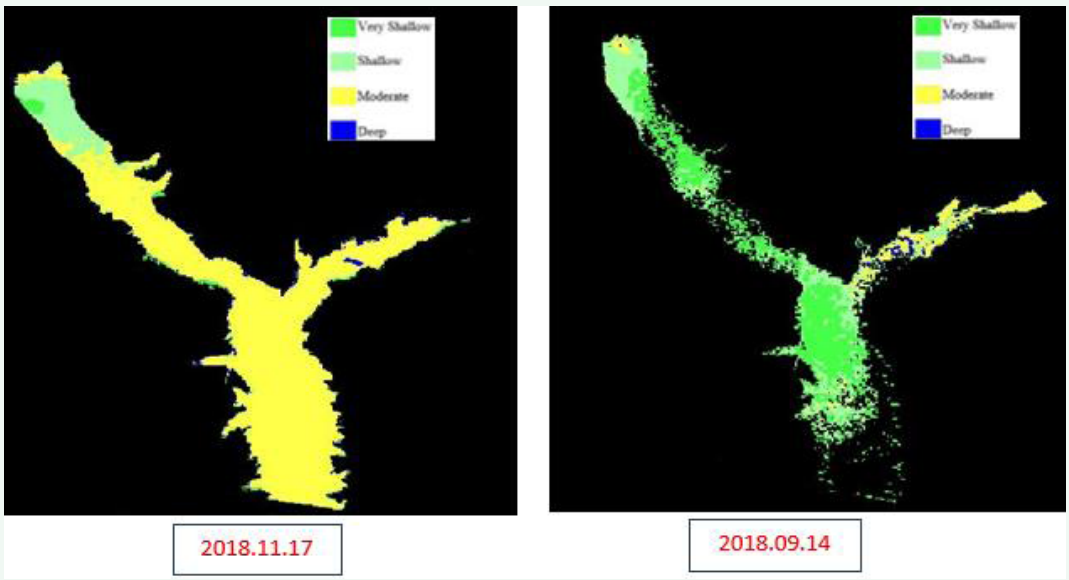

Figure 3 Sample of water depth changes.

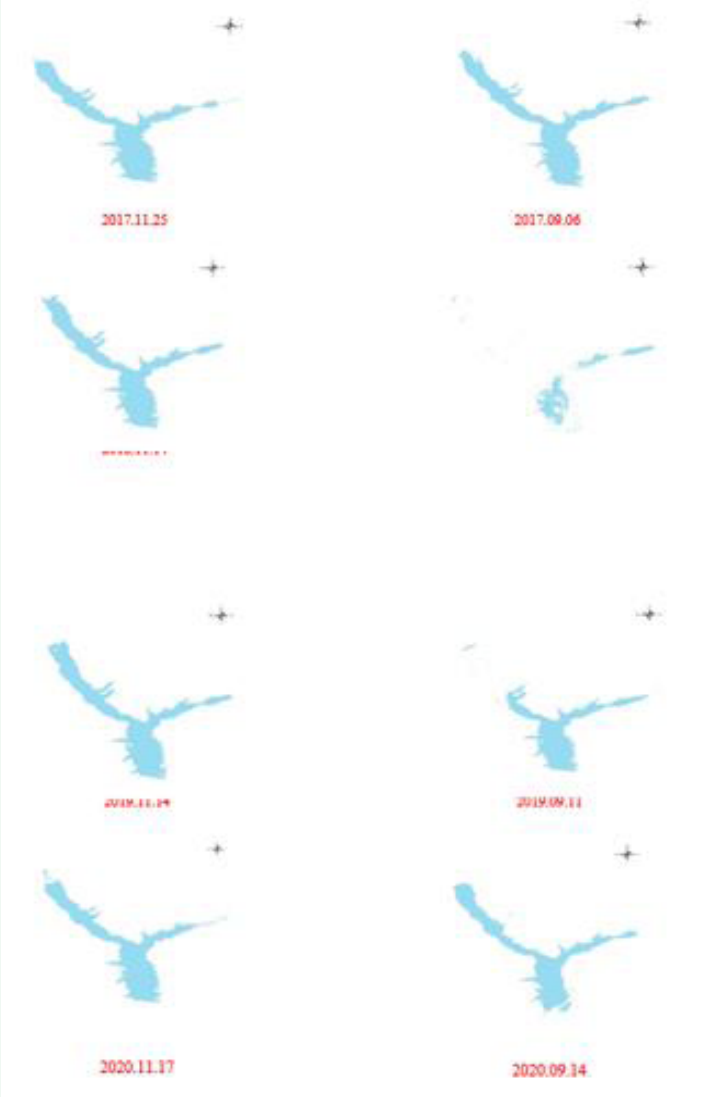

Figure 4 Water body area using Landsat-8 satellite images with MNDWI index from 2015 to 2018 for different months.

Table 2: Comparing the water area of different years with 2020 in two periods of drought and wet years.

Drought Year		
Year	**Percentage increase of water area compared to 2020**	**Percentage reduction of water area compared to 2020**
2017.09.06-2020.09.14	24	
2018.09.24-2020.09.14		60.5
2019.09.11-2020.09.14	22.5	
Wet Year		
2017.11.25-2020.11.17	6.5	
2018.11.14-2020.11.17	18.7	
2019.11.14-2020.11.17	23.4	

Table 3: Amount of area covered for different depths in the lake surface.

NO	Date	Very Shallow	Shallow	Moderate	Deep
1	2017.09.06	2.3913	1.2615	0.4938	0.0456
2	2017.11.25	1.1126	3.8232	0.2110	0.0247
3	2018.09.24	0.1851	0.002	0.0101	0.006
4	2018.11.14	0.3057	3.8639	1.63	0.064
5	2019.09.11	2.9835	0.9643	0.2254	0.0429
6	2019.11.14	3.400	2.4813	0.3980	0.060
7	2020.09.14	1.559	1.007	0.3694	0.0396
8	2020.11.17	0.1392	0.5136	4.059	0.066

during the drought period. The values of depth changes by area for four very shallow, shallow, medium, and deep conditions for different months from 2017 to 2020 are given in (Table 3). The largest depth coverage area, for the very shallow state, is related to the date of 2017.11.14, which is 3.4 km^2. For the shallow state, its value is 3.8639 km^2 on 2018.11.14. Also, the water area

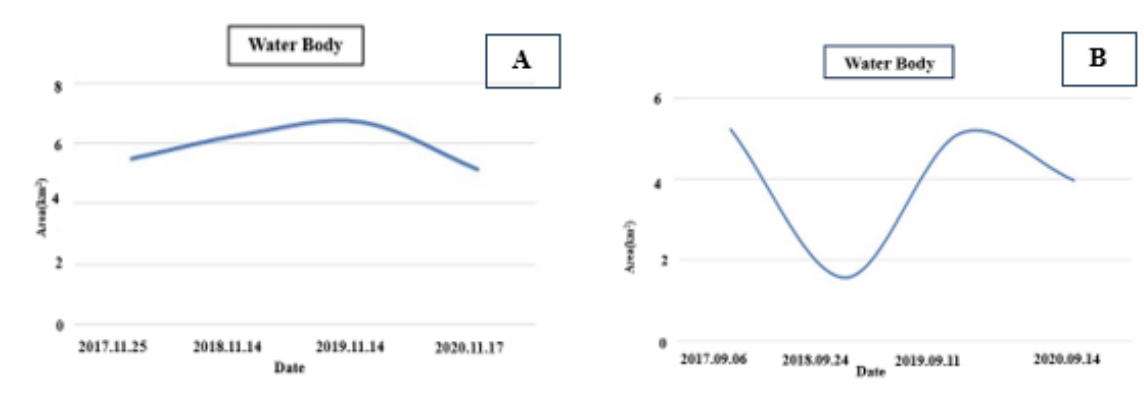

Figure 5 Changes in the area of the water body. A fall period and B summer period.

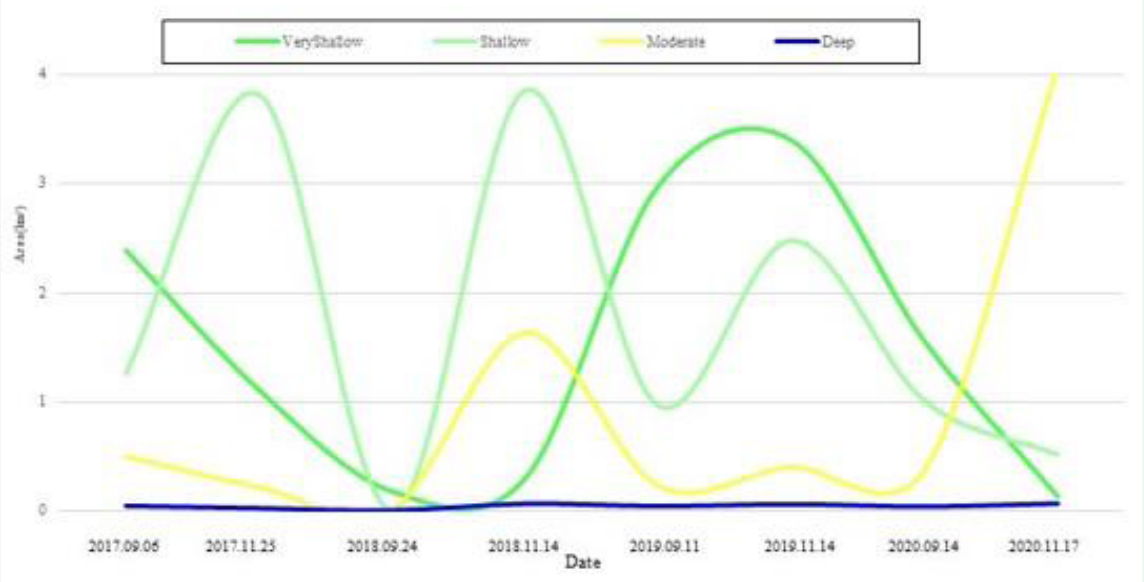

Figure 6 Graph of water depth area changes from 2017 to 2020.

covered for the medium state is 4.059 km^2 as of 2020.11.17 and finally, for the deep state, its area is 0.066 km^2 as of 2020.11.17. Also, (Figure 6) shows the amount of water depth changes for four states from 2017 to 2020. As shown in (Figure 6), the lowest amount of fluctuation is related to the deep state, which has the lowest number of changes.

CONCLUSION

In this study, changes in the water area of the Malo dam lake as well as depth changes were investigated using Landsat 8 satellite images. Also, image fusion has been used to increase the power of spatial resolution using remote sensing techniques. According to the studies obtained, the amount of water area decreased from 2017 to 2020, which indicates the lack of precipitation, especially in the spring and summer seasons. The lowest amount of water area in the studied period is related to the date of 2018.09.24, which is 1.5654 km^2. The reason for this can be pointed to the severe lack of precipitation in spring and summer, as well as the increase in temperature and, naturally, the increase in water evaporation and the increase in water consumption in hot seasons. In this research, the MNDWI index was used to estimate the amount of water area, which largely separates the water area from other complications, the reason is that the amount of moisture in this index is ignored in the estimation of the water area. Considering that in the last 11 years, we have not had a single disaster in this area and the underground water resources and the water behind the dam have decreased drastically, for this

purpose, calculating the amount of water stored and the water area behind the dam is of great importance. In this article, only using Landsat 8 satellite images and the fusion these images from 30 meters to 15 meters, the area of the water area has been estimated. Among other factors that influence the amount of water area, is the ambient temperature, Ambient temperature is one of the factors that influence the amount of water evaporation, and consequently, it can affect the extent of water area. Higher temperatures generally lead to increased evaporation rates, resulting in a reduction of water surface area., which can be investigated and analyzed in future research.

COMPETING INTERESTS STATEMENT

The authors declare that they have no known competing financial interests or personal relationships that could have appeared to influence the work reported in this paper.

Conflict of Interest: We have no conflict of interest to declare. "No funding was obtained for this study".

REFERENCES

1. Aarninkhof SGJ, Ruessink BG, Roelvink JA. Nearshore subtidal bathymetry from time-exposure video images. Journal of Geophysical Research: Oceans. 2005; 110(C6).
2. Anim DO, Kabo-bah AT, Nkrumah PN, Murava RT. Evaluation of NDVI using Spot-5 satellite data for northern Ghana. Environmental Management and Sustainable Development. 2013; 2(1): 167.
3. Bell PS. Shallow water bathymetry derived from an analysis of X-band marine radar images of waves. Coastal Engineering. 1999; 37(3-4): 513-527.
4. Brown S, Versace VL, Laurenson L, Ierodiaconou D, Fawcett J, Salzman S. Assessment of spatiotemporal varying relationships between rainfall, land cover and surface water area using geographically weighted regression. Environmental Modeling & Assessment. 2012; 17: 241-254.
5. Castellanos-Quiroz HOA, Ramírez-Daza HM, Ivanova Y. Detection of open-pit mining zones by implementing spectral indices and image fusion techniques. Dyna. 2017; 84(201): 42-49.
6. Daza RJM, Gonzalez LCB, Leon JCM. Improving the spatial resolution of Ikonos images based on orthophotos: an application of image fusion with wavelet transform. In 2016 11th Iberian Conference on Information Systems and Technologies (CISTI). 2016; 1-6.
7. Dennison PE, Roberts DA, Peterson SH, Rechel J. Use of normalized difference water index for monitoring live fuel moisture. International journal of remote sensing. 2005; 26(5): 1035-1042.
8. Du Y, Zhang Y, Ling F, Wang Q, Li W, Li X. Water bodies' mapping from Sentinel-2 imagery with modified normalized difference water index at 10-m spatial resolution produced by sharpening the SWIR band. Remote Sensing. 2016; 8(4): 354.
9. Ebrahimi Kia M, Saadat Seresht M, Firouz B. Evaluation of bathymetry methods using satellite data. In Geomatic conference, Iran, Tehran. 2009.
10. ED Chaves M, CA Picoli M, Sanches, ID. Recent applications of Landsat 8/OLI and Sentinel-2/MSI for land use and land cover mapping: A systematic review. Remote Sensing. 2020; 12(18): 3062.
11. Fisher A, Flood N, Danaher T. Comparing Landsat water index methods for automated water classification in eastern Australia. Remote Sensing of Environment. 2016; 175: 167-182.
12. Geyman EC, Maloof AC. A simple method for extracting water depth from multispectral satellite imagery in regions of variable bottom type. Earth and Space Science. 2019; 6(3): 527-537.
13. Halabisky M, Moskal LM, Gillespie A, Hannam M. Reconstructing semi-arid wetland surface water dynamics through spectral mixture analysis of a time series of Landsat satellite images (1984-2011). Remote sensing of environment. 2016; 177: 171-183.
14. Hansen MC, Loveland TR. A review of large area monitoring of land cover change using Landsat data. Remote sensing of Environment. 2012; 122: 66-74.
15. Holman R, Plant N, Holland T. cBathy: A robust algorithm for estimating nearshore bathymetry. Journal of geophysical research: Oceans. 2013;118(5): 2595-2609.
16. Ji L, Zhang L, Wylie B. Analysis of dynamic thresholds for the normalized difference water index. Photogrammetric Engineering & Remote Sensing. 2009; 75(11): 1307-1317.
17. Laben CA, Brower BV. U.S. Patent No. 6,011,875. Washington, DC: U.S. Patent and Trademark Office. 2000.
18. Ma S, Tao Z, Yang X, Yu Y, Zhou X, Li Z. Bathymetry retrieval from hyperspectral remote sensing data in optical-shallow water. IEEE Transactions on Geoscience and Remote Sensing. 2013; 52(2): 1205-1212.
19. Malmir M, Zarkesh MMK, Monavari SM, Jozi SA, Sharifi E. Urban development change detection based on Multi-Temporal Satellite Images as a fast tracking approach-a case study of Ahwaz County, southwestern Iran. Environmental monitoring and assessment. 2015; 187: 1-10.
20. Medina J, González LB, Upegui E. Spectral and spatial assessment of the Ikonos images fusion, using the Principal Components, Brovey Transform and Multiplicative. In 2019 14th Iberian Conference on Information Systems and Technologies (CISTI). 2019; 1-6.
21. Ouma YO, Tateishi R. A water index for rapid mapping of shoreline changes of five East African Rift Valley lakes: an empirical analysis using Landsat TM and ETM+ data. International Journal of Remote Sensing. 2006; 27(15): 3153-3181.
22. Ovakoglou G, Alexandridis TK, Crisman TL, Skoulikaris C, Vergos GS. Use of MODIS satellite images for detailed lake morphometry: Application to basins with large water level fluctuations. International journal of applied earth observation and geoinformation. 2016; 51: 37-46.
23. Purkis SJ, Klemas VV. Remote sensing and global environmental change. John Wiley & Sons. 2011.
24. Rajabi AM, Ghorbani E. Land subsidence due to groundwater withdrawal in Arak plain, Markazi province, Iran. Arabian Journal of Geosciences. 2016; 9: 1-7.
25. Rodrigues SC, Silva TI. Dam construction and loss of geodiversity in the Araguari river basin, Brazil. Land Degradation & Development. 2012; 23(4): 419-426.
26. Roohi M, Faeli M, Irani M, Shamsaei E. Calculation of land subsidence and changes in soil moisture and salinity using remote sensing techniques. Environmental Earth Sciences. 2021; 80(12): 423.
27. Roohi M, Faeli M, Jamshidi F, Ghasroddashti AP. Snow parameters modeling using remote sensing techniques and HEC-HMS hydrological modeling-case study: Kan Basin. Environ Monit Assess. 2023; 195(6): 684. doi: 10.1007/s10661-023-11326-2. PMID: 37193863.
28. Roohi M, Soleymani K, Salimi M, Heidari M. Numerical evaluation of the general flow hydraulics and estimation of the river plain by solving the Saint-Venant equation. Modeling Earth Systems and Environment. 2020; 6: 645-658.

29. Shahtahmassebi A, Yang N, Wang K, Moore N, Shen Z. Review of shadow detection and de-shadowing methods in remote sensing. Chinese geographical science. 2013; 23: 403-420.

30. Su H, Liu H, Wu Q. Prediction of water depth from multispectral satellite imagery-the regression Kriging alternative. IEEE Geoscience and Remote Sensing Letters. 2015; 12(12): 2511-2515.

31. Van Dongeren A, Plant N, Cohen A, Roelvink D, Haller MC, Catalán P. Beach Wizard: Nearshore bathymetry estimation through assimilation of model computations and remote observations. Coastal engineering. 2008; 55(12): 1016-1027.

32. Wilson CO. Land use/land cover water quality nexus: quantifying anthropogenic influences on surface water quality. Environ Monit Assess. 2015; 187(7): 424. doi: 10.1007/s10661-015-4666-4. Epub 2015 Jun 12. PMID: 26065891.

33. Xie H, Luo X, Xu X, Pan H, Tong X. Evaluation of Landsat 8 OLI imagery for unsupervised inland water extraction. International Journal of Remote Sensing. 2016; 37(8): 1826-1844.

34. Xu H. Modification of normalised difference water index (NDWI) to enhance open water features in remotely sensed imagery. International journal of remote sensing. 2006; 27(14): 3025-3033.

35. Xu H. Extraction of urban built-up land features from Landsat imagery using a thematicoriented index combination technique. Photogrammetric Engineering & Remote Sensing. 2007; 73(12): 1381-1391.

36. Yang K, Li M, Liu Y, Cheng L, Huang Q, Chen Y. River detection in remotely sensed imagery using Gabor filtering and path opening. Remote Sensing. 2015; 7(7): 8779-8802.

37. Yang Y, Liu Y, Zhou M, Zhang S, Zhan W, Sun C, et al. Landsat 8 OLI image based terrestrial water extraction from heterogeneous backgrounds using a reflectance homogenization approach. Remote Sensing of Environment. 2015; 171: 14-32.

38. Young NE, Anderson RS, Chignell SM, Vorster AG, Lawrence R, Evangelista PH. A survival guide to Landsat preprocessing. Ecology. 2017; 98(4): 920-932. doi: 10.1002/ecy.1730. Epub 2017 Mar 20. Erratum in: Ecology. 2021; 102(11): e03508. PMID: 28072449.